ECS Transactions, 85 (13) 729-734 (2018)
10.1149/08513.0729ecst ©The Electrochemical Society

Internal Photoemission Spectroscopy Measurements of the Energy Barrier Heights between ALD SiO_2 and Ta-based Amorphous Metals

M.A. Jenkins, T. Klarr, J.M. McGlone, J.F. Wager, and J.F. Conley, Jr.
School of Electrical Engineering and Computer Science, Oregon State University
Corvallis, Oregon 97331

Internal photoemission spectroscopy is used to measure energy barrier heights in metal/insulator/metal (MIM) structures with plasma-enhanced atomic layer deposited SiO_2 and amorphous metals TaWSi and TaNiSi and polycrystalline TaN bottom electrodes. With an Al top electrode, the TaWSi/SiO_2 barrier height is 4.0 eV. Al and Au barrier heights with SiO_2 were found to be 3.7 eV and 4.2-4.3 eV, respectively. With a Au top electrode, barrier heights between SiO_2 and Ta-based bottom electrodes could not be reliably extracted. The Au top electrode device with a TaWSi bottom electrode exhibited switching behavior, pointing towards migration of a positively charged species in the dielectric which was not observed with the Al top electrode.

Introduction

Metal/insulator/metal (MIM) tunnel diodes are of interest for use in high-speed applications such as rectenna based energy harvesting of IR radiation, as building blocks for beyond CMOS hot-electron (MIMIM) transistors, and for use in resistive random access memory (1–3). Tunnel diodes ideally operate via Fowler-Nordheim tunneling (FNT), which is strongly dependent both on electric field and the height of the energy barriers between the two metal electrodes and the insulator. As such, a very smooth bottom electrode is necessary to provide a uniform electric field and charge transport throughout the MIM device. Amorphous metals are excellent candidates for this application as they are atomically smooth due to their amorphous nature. The amorphous metal ZrCuAlNi has been previously shown to function well as a bottom electrode for MIM devices (4–6), but suffers from an interfacial oxide and thermal instability above ~300 °C. Recently, Ta-based amorphous metals such as TaWSi and TaNiSi have been shown to have larger work functions and stability approaching 900 °C and above (7).

Because FNT is strongly dependent on the metal/insulator barrier heights in the device, knowledge of these barrier heights is critical for predicting, understanding, and optimizing MIM diode device operation. The Schottky-Mott model may be used to predict ideal barrier heights ($\varphi_{Bn} = \Phi_M - \chi_i$) from the metal vacuum work function (Φ_M) and insulator electron affinity (χ_i). However, actual barrier heights depend strongly on deposition method and interface properties and often differ substantially from ideal values. Internal photoemission (IPE) spectroscopy may be used to directly measure barrier heights at interfaces buried within the device of interest. In this work, IPE is utilized to measure the metal/insulator barrier heights in MIM stacks with Ta-based amorphous metal bottom electrodes or polycrystalline TaN, using both Au and Al as top electrodes.

Experimental

MIM devices were fabricated on silicon substrates with 100 nm of thermally grown SiO_2 to provide electrical isolation from the underlying silicon. TaWSi and TaNiSi bottom electrodes were deposited using DC magnetron sputtering from single alloy targets (7, 8). TaN bottom electrodes (obtained from ON Semiconductor) consisted of a $Si/SiO_2/Ta/TaN$ stack that was planarized via chemical-mechanical planarization. SiO_2 was deposited on the bottom electrodes with plasma-enhanced atomic layer deposition (PEALD) using bis(diethylamino)silane (BDEAS) and O_2 plasma as precursors in a Picosun SUNALE R-200 reactor at 200 °C. The targeted dielectric thickness was 15 nm. For the semi-transparent top contact needed for IPE measurements, approximately 10 nm of either Al or Au was deposited via thermal evaporation. Au top electrodes were patterned with a shadow mask to yield circular devices with a diameter of 250 μm. Al top electrodes were patterned with photolithography into 200 by 200 μm squares.

IPE measurements were conducted using a 150 W Xe arc lamp light source passed through a monochromator, followed by a long-pass filter to remove second-order diffraction. The light was then shined onto the device of interest using a parabolic mirror focused to a spot size of 1 mm^2. Electrical bias was applied to the bottom electrode and the top electrode was held at ground. At each applied bias, the current was measured as the photon energy ($h\nu$) was swept from 2 to 5 eV.

Results and Discussion

Procedure for barrier height determination

Current was normalized for each applied bias, such that only the light-induced current (I_{ph}) was analyzed. The quantum yield (Y) was then calculated using Eqn. 1,

$$Y = (I_{ph} * h\nu) / P_{ph} \quad [1]$$

where P_{ph} is the power of the light incident on the sample, as measured by a silicon photodiode.

The next step in data analysis was to determine spectral thresholds (Φ_{thresh}) from plots of $Y^{1/2}$ versus $h\nu$ (9, 10), where $Y^{1/2}$ was used to account for the energy distribution at a metal interface. Spectral thresholds were found using an algorithm to find the largest region of the $Y^{1/2}$ curve with the highest linearity, as determined from the R^2 value of a linear regression. Once the region for linearization was determined, the x-intercept was calculated, giving Φ_{thresh} for that specific bias. Φ_{thresh} extractions for SiO_2 devices with Al and Au top electrodes and Ta-based bottom electrodes are shown in Figure 1. It must be noted that with a Au top electrode, barrier heights between SiO_2 and the Ta-based metals were not extracted due to difficulty in finding repeatable linear regions for spectral threshold extractions, which will be discussed later. The built-in field for each device was determined as an average of the crossover point of I_{ph} from a positive to negative value over the range of $h\nu$. Φ_{thresh} were then plotted as a function of the square root of the electric field in the oxide ($\xi^{1/2}$), taking into account the built-in field in the device. The y-intercept of a linear regression of this data was then found in order to obtain the zero-field barrier height, $\varphi_{bn\text{-}0}$, to account for field-dependent barrier lowering (11). This extraction is shown for SiO_2 devices in Figure 2. Ideally, this field dependence is due to image-force barrier lowering, and the slope of the extraction is dependent on the dielectric constant of

the oxide. However, that was not the case for these extractions. This non-ideality may be due the presence of charges near the interface or interfacial layers, and is typically reported for metal-insulator barriers (12–14).

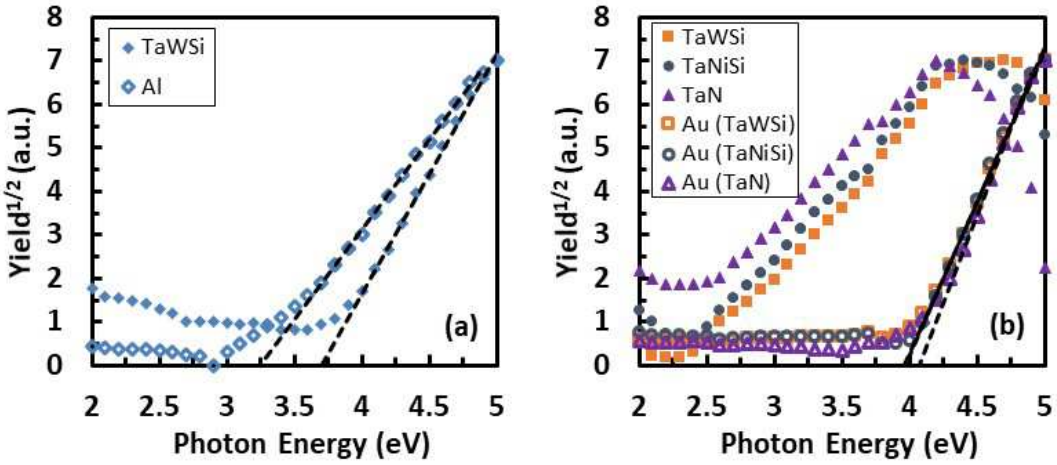

Figure 1. Representative spectral threshold extractions for devices with (a) Al and (b) Au top electrodes. Dashed lines show the extracted spectral threshold for each interface. Note that barriers were not extracted for the SiO_2 and bottom electrode interfaces for the Au devices.

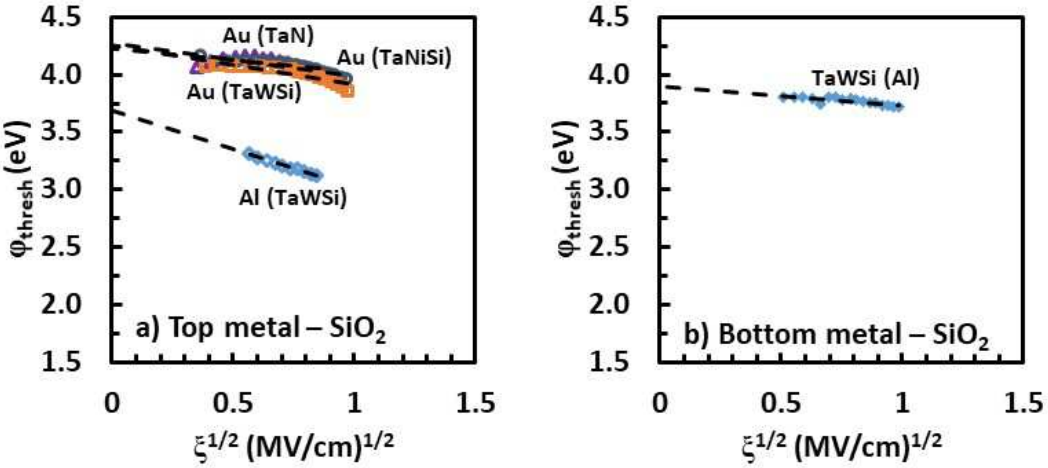

Figure 2. Schottky plots used to extrapolate the zero-field barrier height from IPE-derived spectral thresholds.

SiO_2 Barrier Heights with Ta-based Metals

First, SiO_2 was characterized with an Al top electrode and TaWSi bottom electrode to directly compare to previous work with ZrCuAlNi (12). This yielded a similar Al barrier at 3.7 eV, and a TaWSi barrier height of 4.0 eV, larger than the ZrCuAlNi barrier height of 3.3 eV (12). This is in agreement with Kelvin probe measurements that indicate TaWSi has a larger vacuum work function than ZrCuAlNi (15, 16).

To avoid the potential for oxidation of the top electrode, Au was used as the top electrode when comparing the bottom electrodes in this study. Bottom electrodes of

TaWSi, TaNiSi, and TaN were studied. The Au barrier height measured for all three bottom electrodes was between 4.2-4.3 eV, within experimental error of one another. This suggests that the bottom electrode is not impacting the barrier height of the top electrode. This value is ~0.6 eV greater than the Al barrier height, where a difference of ~0.9 eV would be expected from the vacuum work function difference between Au and Al. The expected barrier height between Au (Φ_M = 5.2 eV) and SiO_2 (χ_i = 0.9 eV) is 4.3 eV, which matches the measured barrier height. These two observations support previous reports of a dipole at the interface of ALD insulators and Al that increases the barrier height between Al and the ALD insulator (14).

A clear, consistent region of linearity could not be determined for spectral threshold extractions for the barrier height between SiO_2 and Ta-based metals when a Au top electrode was used. However, the zero-field barrier height from the spectral thresholds that could be extracted yielded a value far lower than expected. The TaWSi barrier height was over 1 eV lower than was measured with an Al top electrode. A potential explanation for this lower than expected TaWSi barrier height is the presence of charge at the TaWSi interface.

In previous work with Ta-based metals, it was postulated that negative Ta ion migration into an ALD oxide following a post-deposition anneal could lead to an increase in barrier height (17). This is the opposite effect of what was observed in this work. However, it is possible that positive Au ion migration to the opposing electrode could cause a lower TaWSi barrier height than expected. Au is known to migrate through oxides, and may even be used to form conductive bridges that display switching behavior as in conductive bridging random access memory (CBRAM) (18, 19). IPE determination of the bottom electrode barrier height in this work is performed with a positive bias applied to the top electrode over a relatively long period of time, giving ample time for positively charged Au ions to migrate to the opposing electrode. These positively charged Au ions could cause a lowering of the barrier height at the bottom electrode.

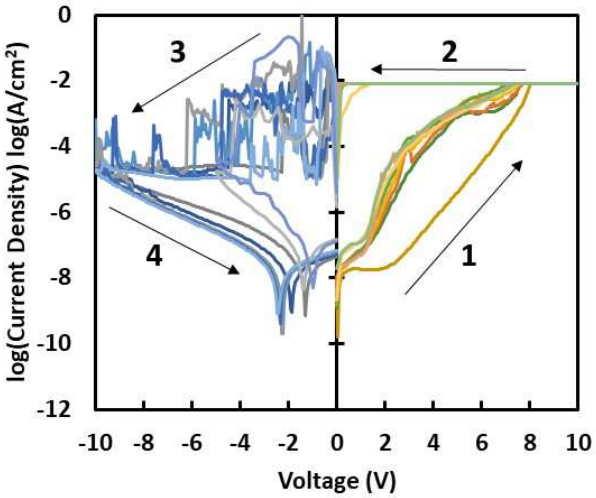

Figure 3. Switching behavior exhibited by Au/SiO_2/TaWSi device over 9 cycles.

Significant Au migration would likely lead to switching behavior. IV measurements were used to look for switching behavior in TaWSi bottom electrode devices. Of those tested, only the Au/SiO_2/TaWSi device exhibited reversible resistance switching of the device, shown in Figure 3, while the SiO_2 device with an Al top electrode did not. The

migration of Au would explain why only the Au top electrode device exhibits switching behavior and why a clear, repeatable linear region could not be found for spectral threshold extraction for the SiO_2/Ta-based metal interface when using a Au top electrode.

Conclusion

The barrier height between PEALD SiO_2 and TaWSi was determined, with a comparison made between Al and Au top electrodes. Samples with TaWSi, TaNiSi, or TaN bottom electrodes and Au top electrodes yielded a Au barrier height between 4.2-4.3 eV. Reliable bottom electrode barrier height extractions could not be made for samples with Au top electrodes due to a lack of consistent linear regions in the yield curve for spectral threshold extraction. However, the spectral thresholds that were extracted were much lower than with an Al top electrode. The presence of positive ions near the interface of the Ta-based metals could explain this lower barrier height, one example of which would be Au migration from the top electrode, as evidenced by observable resistive switching behavior. A comparison to previous work with ZrCuAlNi showed that TaWSi has a larger work function than ZrCuAlNi. Due to its low roughness and significantly higher temperature stability than ZrCuAlNi, TaWSi may be promising for use as a high work function bottom electrode in MIM tunnel diodes.

Acknowledgments

This work is supported by NSF Center for Sustainable Materials Chemistry, grant CHE-1102637. The authors thank C. Tasker for equipment support. This work was conducted at the Materials Synthesis and Characterization (MaSC) Center, a National Nanotechnology Coordinated Infrastructure (NNCI) Northwest Nanotechnology Infrastructure (NWNI) user facility at Oregon State University, which is supported in part by the National Science Foundation (Grant ECC-1542101) and Oregon State University.

References

1. G. Moddel and S. Grover, *Rectenna solar cells*, Springer Science & Business Media, New York, (2013).
2. S. Vaziri, A. D. Smith, M. Östling, G. Lupina, J. Dabrowski, G. Lippert, W. Mehr, F. Driussi, S. Venica, V. Di Lecce, A. Gnudi, M. König, G. Ruhl, M. Belete, and M. C. Lemme, *Solid State Commun.*, **224**, 64–75 (2015).
3. D. Ielmini, *Semicond. Sci. Technol.*, **31**, 63002 (2016).
4. N. Alimardani, S. W. King, B. L. French, C. Tan, B. P. Lampert, and J. F. Conley, Jr., *J. Appl. Phys.*, **116**, 24508 (2014).
5. N. Alimardani, E. W. Cowell, J. F. Wager, J. F. Conley, Jr., D. R. Evans, M. Chin, S. J. Kilpatrick, and M. Dubey, *J. Vac. Sci. Technol. A*, **30**, 01A113 (2012).
6. N. Alimardani and J. F. Conley, Jr., *Appl. Phys. Lett.*, **102**, 143501 (2013).
7. J. M. McGlone, K. R. Olsen, W. F. Stickle, J. E. Abbott, R. A. Pugliese, G. S. Long, D. A. Keszler, and J. F. Wager, *MRS Commun.*, **7**, 715–720 (2017).
8. J. M. McGlone, K. R. Olsen, W. F. Stickle, J. E. Abbott, R. A. Pugliese, G. S. Long, D. A. Keszler, and J. F. Wager, *J. Alloys Compd.*, **650**, 102–105 (2015).
9. V. V. Afanas'ev and A. Stesmans, *J. Appl. Phys.*, **102**, 81301 (2007).
10. N. V. Nguyen, O. Kirillov, H. D. Xiong, and J. S. Suehle, in *AIP Conference Proceedings*,, vol. 931, p. 308–314, AIP Publishing (2007).

11. R. J. Powell, *J. Appl. Phys.*, **41**, 2424–2432 (1970).
12. M. A. Jenkins, T. Klarr, D. Z. Austin, W. Li, N. V. Nguyen, and J. F. Conley, Jr., *Phys. Status Solidi RRL – Rapid Res. Lett.*, **12**, 1700437 (2018).
13. N. V. Nguyen, H. D. Xiong, J. S. Suehle, O. A. Kirillov, E. M. Vogel, P. Majhi, and H.-C. Wen, *Appl. Phys. Lett.*, **92**, 92907 (2008).
14. V. V. Afanas'ev, M. Houssa, A. Stesmans, and M. M. Heyns, *J. Appl. Phys.*, **91**, 3079–3084 (2002).
15. J. M. McGlone, thesis, Oregon State University (2014).
16. E. W. Cowell, N. Alimardani, C. C. Knutson, J. F. Conley, Jr., D. A. Keszler, B. J. Gibbons, and J. F. Wager, *Adv. Mater.*, **23**, 74–78 (2011).
17. S. Shamuilia, V. V. Afanas'ev, A. Stesmans, T. Schram, and L. Pantisano, *J. Appl. Phys.*, **104**, 73722 (2008).
18. J. G. Simmons and R. R. Verderber, *Proc R Soc Lond A*, **301**, 77–102 (1967).
19. C.-N. Peng, C.-W. Wang, T.-C. Chan, W.-Y. Chang, Y.-C. Wang, H.-W. Tsai, W.-W. Wu, L.-J. Chen, and Y.-L. Chueh, *Nanoscale Res. Lett.*, **7**, 559 (2012).